

FIRST-PRINCIPLES INVESTIGATION OF ELECTRONIC AND NONLINEAR OPTICAL PROPERTIES OF LINBO₃ FOR HIGH-SPEED FIBER-OPTIC COMMUNICATION APPLICATIONS**Priyanka Singh¹ and Mulayam Singh Patel^{1*}**¹Department of Physics, Nehru Gram Bharati (Deemed to be University), Prayagraj, Uttar Pradesh, India –221505

*Corresponding Authors' E-mail:

Dr. Mulayam Singh Patel: mulayamsinghau@gmail.comPriyanka Singh: 95pssingh@gmail.com**ABSTRACT**

First-principles DFT calculations were used to study the electronic and optical properties of LiNbO₃. The band structure shows a clear wide band gap with no states at the Fermi level, confirming its insulating nature. The valence bands are dominated by localized O-2p states, while the dispersive Nb-4d conduction bands enable efficient optical excitations. The total density of states supports these features, with prominent peaks linked to flat bands. Optical properties derived from the dielectric function reveal a high refractive index (3.37) near the absorption edge, indicating strong polarization and light-matter interaction. Low absorption in the visible region confirms optical transparency, whereas intense ultraviolet absorption and conductivity peaks arise from interband transitions. The energy loss function exhibits a strong plasmon resonance around 25–26 eV, reflecting collective electronic excitations. Overall, the results highlight the excellent optical stability and strong electronic response of LiNbO₃, making it highly suitable for nonlinear optics, electro-optic modulation, and fiber-optic communication applications.

Keywords:LiNbO₃; Density Functional Theory; Fiber Optics; Refractive Index; Nonlinear optics**1. Introduction**

The rapid expansion of high-speed fiber-optic communication networks has created an unprecedented demand for materials capable of supporting fast, energy-efficient, and broadband photonic signal processing. As data traffic continues to rise exponentially, driven by 5G/6G connectivity, cloud computing, and quantum communication infrastructures, photonic components must exhibit superior electro-optic, nonlinear optical (NLO), and transmission characteristics to meet modern performance requirements. Lithium niobate (LiNbO₃), a well-established ferroelectric oxide, has re-emerged as a leading platform for next-generation integrated photonics due to its exceptional NLO coefficients, wide transparency window, and compatibility with chip-scale fabrication techniques [1–6]. Despite decades of technological maturity, recent breakthroughs in thin-film engineering, defect control, and heterogeneous integration have further renewed interest in understanding LiNbO₃ from an electronic-structure perspective, particularly using first-principles approaches.

LiNbO₃ possesses a rhombohedral (R3c) ferroelectric structure characterized by spontaneous polarization originating from Nb-O octahedral distortions [2, 4]. Its crystal stability, domain behavior, and defect chemistry critically influence its optical response, making accurate electronic-structure studies indispensable for device optimization. Early studies have established the fundamental structural parameters and ferroelectric nature of LiNbO₃ [4], while more recent density functional theory (DFT) investigations have shed light on defect energetics, band-structure modifications, and polarization-driven electronic behavior [5]. However, significant discrepancies remain in experimentally reported band-gap values and optical constants, largely due to defects, stoichiometry variations, and dopant incorporation, which can strongly modify absorption characteristics and refractive-index dispersion [6-18]. Therefore, a rigorous first-principles investigation is essential to quantify intrinsic electronic properties and their relationship with nonlinear optical phenomena.

The nonlinear optical capabilities of LiNbO₃ are central to its role in photonic communication systems. Its large second-order susceptibility (χ^2) and strong electro-optic (Pockels) coefficient have long been exploited in modulators, parametric converters, and frequency mixers [1]. Classical optical textbooks highlight LiNbO₃ as

one of the most versatile and efficient NLO crystals available [1]. Detailed experimental work has further characterized its electro-optic response, domain control, and refractive-index behavior under different temperatures and wavelengths [6, 7]. These properties have enabled the realization of tunable microring resonators [11], integrated electro-optic modulators [12], low-loss waveguides [19], and advanced fiber couplers [27] essential for high-speed communication links.

Recent advancements in LiNbO₃ photonics have focused on monolithic and heterogeneous integration of thin-film LiNbO₃ (TFLN), which significantly enhances modulation bandwidth, reduces device footprint, and lowers propagation losses [10, 14]. For instance, hybrid silicon–LiNbO₃ architectures integrate the strong electro-optic effects of LiNbO₃ with efficient silicon waveguiding, enabling compact and high-performance optical links [20]. Progress in thin-film fabrication has also led to record-low optical losses and ultrafast modulation speeds suitable for terahertz-scale communication systems [13, 21]. Beyond classical telecommunications, LiNbO₃ has become a cornerstone for quantum photonics, allowing on-chip entangled-photon generation, frequency-comb formation, and microwave-to-optical conversion [9, 15, 16, 22]. These emerging applications further emphasize the need for precise knowledge of intrinsic material properties, particularly those governing electronic transitions and NLO susceptibilities.

Accurate optical response and electrical structure prediction through first-principles theory provides critical insights that guide photonic device engineering. DFT-based studies have analyzed the band dispersion, optical conductivity, and dielectric behavior of LiNbO₃ [3, 8, 20]. These investigations have revealed anisotropic electronic transitions linked to its ferroelectric distortion, providing a theoretical explanation for observed optical birefringence and absorption spectra. Moreover, band-gap engineering via chemical doping or defect control has demonstrated the ability to tailor transparency and enhance NLO efficiency, making first-principles simulations an essential tool for next-generation device design [18, 23]. Despite these efforts, a unified first-principles understanding that links electronic-structure features—such as band-gap character, orbital contributions, and polarization effects—to nonlinear optical coefficients remains limited.

The role of defects is particularly significant. Lithium vacancies, niobium antisite defects, and oxygen vacancies not only alter the electronic band structure but also strongly impact optical absorption, domain stability, and waveguide performance [5, 17, 24]. Recent spectroscopy studies have confirmed that defect-induced states in the band gap are responsible for UV-induced optical absorption and reduced transparency [17]. Similarly, dielectric spectroscopy and optical-conductivity measurements reveal strong correlations between electronic excitations and ferroelectric behavior [25, 26]. Understanding these phenomena from a first-principles perspective can help optimize fabrication processes to suppress detrimental defects and improve transparency for high-speed optical modulators.

In fiber-optic communication, optical losses and bandwidth limitations remain primary challenges for integrated photonic devices. LiNbO₃-based modulators benefit from exceptionally low chromatic dispersion and strong electro-optic coefficients, enabling ultrafast modulation with low insertion loss [12, 27-28]. However, achieving low-loss waveguiding requires precise control over crystalline uniformity, defect concentrations, and interface quality—parameters that are inherently linked to the material's electronic structure [19, 29]. Furthermore, plasmonic enhancements in LiNbO₃ nanostructures demonstrate promising opportunities for subwavelength field confinement and ultrafast optical switching, though their performance remains highly dependent on electronic-transition energies and dielectric response [30-31]. Such innovations underscore the importance of accurate first-principles modeling to predict and optimize nonlinear optical behavior under diverse photonic operating conditions.

Given these considerations, a comprehensive first-principles investigation of LiNbO₃ is vital for advancing its functionality in next-generation fiber-optic communication technologies. By correlating intrinsic electronic properties, defect physics, and NLO characteristics, first-principles methods can help resolve longstanding uncertainties in band-gap estimation, electronic anisotropy, and optical-transition behavior. Furthermore, these insights can guide material design strategies—such as controlled doping, defect engineering, and nanostructuring—to enhance electro-optic performance, reduce optical losses, and maximize nonlinear efficiency. As the field moves toward chip-scale integration of high-speed photonics, an accurate theoretical understanding of LiNbO₃ will be crucial in determining how an optical communication system develops in the future.

2. COMPUTATIONAL DETAILS:

The LiNbO₃ crystal structure underwent DFT analysis via the CASTEP module within Materials Studio software. Calculations relied on the Materials Studio package [32-34], applying the Perdew-Burke-Ernzerhof (PBE) functional under the generalized gradient approximation (GGA) for exchange-correlation treatment. The

Koelling-Harmon method was used to integrate relativistic corrections, and a plane-wave basis was selected at a kinetic energy cutoff of 489.8 eV.

Using a density mixing method, the system was treated as non-metallic for electronic minimization. A total energy tolerance of 0.2×10^{-5} eV/atom and an eigen-energy tolerance of 0.48×10^{-6} eV, with a maximum of 100 SCF cycles, were among the convergence requirements. Stabilizing occupation close to band borders with a Gaussian smearing of 0.1 eV width ensured dependable convergence without compromising accuracy because the small width prevents instabilities.

Density mixing followed a Pulay scheme (history length 20, mixing amplitude 1.5). Band structure computations employed DFT with 41 bands per k-point, capping iterations at 61 (5 steps each).

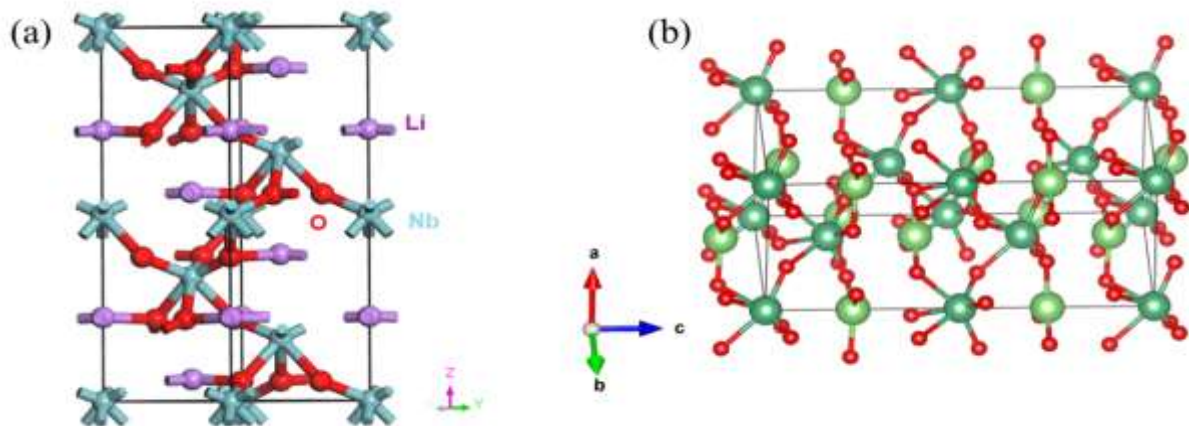


Figure 1: (a) and (b) Structural representations of LiNbO_3 material generated using Materials Studio and VESTA softwares.

3. COMPUTATIONAL RESULT AND DISCUSSION

Figure 2(a) and (b) present the calculated electronic band structure and total density of states (DOS) of LiNbO_3 , providing insight into its electronic behavior. In Figure 2(a), the band structure is shown along high-symmetry directions in k-space, with the Fermi level (E_F) set at 0 eV. No electronic bands cross the Fermi level, confirming that LiNbO_3 is a wide-band-gap semiconducting material. A distinct energy band gap separates the valence band region (below E_F) from the conduction band region (above E_F). The valence bands are relatively flat, indicating localized electronic states that are mainly contributed by O-2p orbitals. In contrast, the conduction bands are more dispersive, reflecting delocalized states primarily originating from Nb-4d orbitals, which facilitate charge transport when excited.

Figure 2(b) shows the total DOS as a function of energy. The DOS is zero at the Fermi level, further confirming the insulating nature of LiNbO_3 . Prominent peaks in the DOS correspond to energy regions where bands are flat in the band structure, indicating a high density of electronic states. The broader features at higher energies arise from overlapping conduction bands. Overall, the agreement between the band structure and DOS provides a consistent picture of the electronic structure of LiNbO_3 and helps explain its optical, dielectric, and nonlinear optical properties.

LiNbO_3 material exhibits exceptional optoelectronic properties, making it an exciting candidate for creating active, multifunctional components within a fiber optic network [2]. Its potential lies in applications that need light

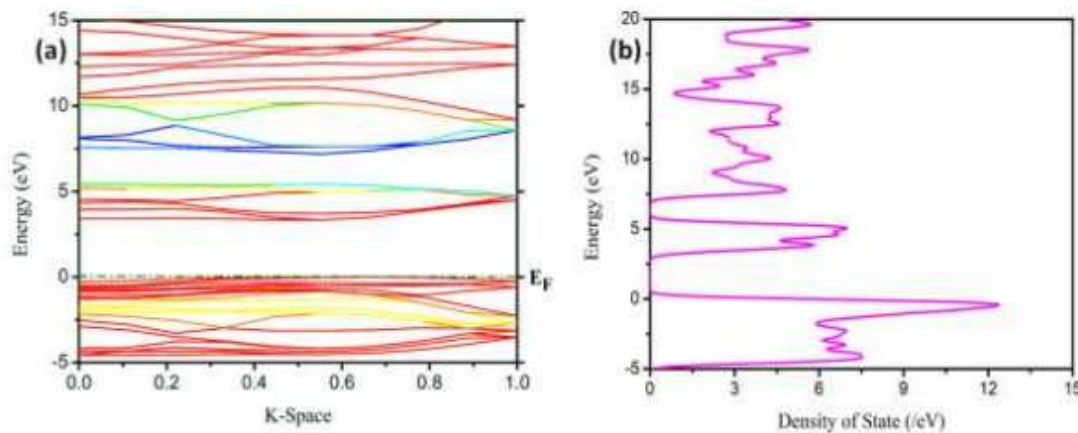


Figure 2. (a) Electronic band structure and (b) total density of states (DOS) of LiNbO₃.

generation, detection, or nonlinear optical modulation, especially those that call for tiny, all-fiber integrated devices.

The behavior of light and its potential for efficient transmission and use are determined by a number of fundamental characteristics in fiber optics. The design and functionality of optical fibers depend heavily on these characteristics, which include refractive index, reflectivity, absorption coefficient, energy loss function, and dielectric function. A material's refractive index, or $n(\omega)$, is a fundamental feature that quantifies how much light slows down as it passes through it. The equation 1 connect the refractive index to the real part $\epsilon_1(\omega)$ and the imaginary part $\epsilon_2(\omega)$ of the dielectric function. Both quantities depend on the angular frequency ω , which corresponds to the frequency of the light wave [33-35].

$$n(\omega) = [\epsilon_1(\omega)/2 + \{\epsilon_1(\omega)^2 + \epsilon_2(\omega)^2\}^{1/2}/2]^{1/2} \quad (1)$$

Total internal reflection (TIR) is the basic process by which light travels through optical fibers. This happens because the refractive index of the fiber core is somewhat greater than that of the surrounding cladding. Light is therefore kept contained within the core and is able to travel great distances with little loss.

The numerical aperture (NA) of the fiber, which determines how well it can gather and direct light, is likewise controlled by the refractive index. Moreover, it has a major impact on dispersion, which is the phenomenon wherein various light wavelengths travel through the fiber at varying speeds.

Figure 3 (a) depict the computational refractive index, $n(\omega)$, for LiNbO₃ as a function of energy. The refractive index is a complex parameter composed of both real and imaginary components, which originate from the corresponding real and imaginary parts of the dielectric function, $\epsilon_1(\omega)$ and $\epsilon_2(\omega)$ respectively. At low photon energies, LiNbO₃ exhibits a relatively high real refractive index, indicating strong light-matter interaction in the transparent region. The maximum value of the real part, approximately 3.37 at 4.22 eV, is associated with strong electronic polarization near the fundamental absorption edge. The imaginary part is nearly zero at low energies, confirming minimal absorption in this region. A pronounced peak in the imaginary component appears around 5.34 eV with a value of about 1.94, corresponding to interband electronic transitions from the valence band to the conduction band.

As energy increases, both real and imaginary parts show oscillatory behavior, reflecting multiple electronic transitions and resonant features in the electronic structure. Beyond ~30 eV, the imaginary part approaches zero, indicating reduced absorption, while the real part gradually stabilizes.

Reflectivity ($R(\omega)$), evaluated using Equation 2, measures how efficiently a material reflects incident light. In fiber-optic systems, low reflectance is preferred—particularly at connectors and splices—to avoid signal loss and degradation. However, reflection at interfaces is unavoidable due to the inherent phenomenon of Fresnel reflection, which must be carefully considered in system design. The reflectivity of the materials is calculated using the standard equation [34-35]:

$$R(\omega) = (n + ik - 1)/(n + ik + 1) \quad (2)$$

$R(\omega)$ quantifies the ability of a material's surface to reflect incident light. Its value varies between 0 and 1, where larger values correspond to stronger reflection. Reflectivity depends on the angular frequency of the incident light (ω) and is governed by the material's complex refractive index ($n + ik$). Here, n represents the real component, which determines the phase velocity of light within the medium, while k , the imaginary

component (extinction coefficient), quantifies the degree of optical absorption.

Figure 3 (b) shows the computed optical reflectivity of LiNbO₃ as a function of photon energy (0–50 eV), obtained from first-principles electronic structure calculations. Reflectivity is directly governed by the complex dielectric function and therefore reflects interband electronic transitions in the material.

In the low-energy region (< 6 eV), the reflectivity is moderate and gradually increases, indicating the onset of optical transitions near the fundamental band gap of LiNbO₃. The pronounced peak at 5.34 eV with a maximum reflectivity of 0.37 corresponds to strong interband transitions, mainly from O-2p valence states to Nb-4d conduction states, which dominate the optical response in this energy range.

Between 6 and 15 eV, multiple smaller peaks and valleys appear, arising from overlapping electronic transitions involving deeper valence bands and higher conduction bands. The reflectivity then decreases significantly around 18–20 eV, indicating reduced optical coupling and increased absorption.

A broad feature around 22–25 eV suggests collective electronic excitations and higher-energy interband transitions. At 30–32 eV, the reflectivity drops close to zero, implying strong absorption and possible plasmon-related damping. A sharp peak near 35–36 eV is attributed to plasmon resonance effects. Beyond 40 eV, reflectivity rapidly diminishes, showing that LiNbO₃ becomes nearly transparent to very high-energy photons.

Equation 3 is used to determine the absorption coefficient ($\alpha(\omega)$), which quantifies how strongly a material absorbs light, resulting in a decrease in signal strength. The absorbance of the substances is computed using the standard relationship [35]:

$$\alpha(\omega) = (2)^{1/2} \omega [\{\varepsilon_1(\omega)^2 + \varepsilon_2(\omega)^2\}^{1/2} - \varepsilon_1(\omega)]^{1/2} \quad (3)$$

Minimizing optical absorption is crucial for efficient long-distance communication. This is accomplished by employing highly purified glass, which forms low-loss transmission windows. Conversely, active optical fibers are deliberately doped with specific additives that absorb light at designated pump wavelengths, thereby enabling signal amplification in fiber amplifiers. Absorption characteristics are also vital in fiber-optic sensors, where variations in a material's absorption in response to external influences are used for detection and measurement.

Figure 3 (c) depicts the computational absorption coefficient, $\alpha(\omega)$, of LiNbO₃ as a function of energy. The absorption coefficient, which is directly correlated with the imaginary component of the dielectric function, measures how strongly incident photons are absorbed by the material.

In the low-energy region (< 4–5 eV), $\alpha(\omega)$ is nearly zero, indicating optical transparency and confirming the wide-band-gap nature of LiNbO₃. A sharp rise in absorption beginning around 5–6 eV marks the onset of interband transitions from O-2p valence states to Nb-4d conduction states. Several pronounced peaks between 7 and 22 eV are observed, reflecting strong and overlapping electronic transitions involving deeper valence bands and higher conduction bands.

A significant reduction in absorption around 25–30 eV suggests a transition to a region with reduced joint density of states. The most intense absorption peak appears at 35.41 eV, reaching a maximum value of $4.2 \times 10^5 \text{ cm}^{-1}$, which can be attributed to collective electronic excitations and plasmon-related transitions. Additional peaks around 38–40 eV further support the presence of high-energy interband and plasmonic effects. Beyond 45 eV, the absorption coefficient decreases substantially and shows weak oscillations up to 70 eV, indicating diminished optical transitions at very high photon energies.

The dielectric function ($\varepsilon(\omega)$) is an intrinsic material parameter that characterizes how a medium responds to an applied external electric field. It is a complex function that varies with the angular frequency of the field. The dielectric function is written as [34-35]:

$$\varepsilon(\omega) = \varepsilon_1(\omega) + i\varepsilon_2(\omega) \quad (4)$$

It's essential for modeling and simulation of light propagation in fibers to understand the relationship between dispersion and absorption via the Kramers-Kronig relations and to explore nonlinear optical phenomena in which the dielectric function becomes intensity-dependent [35]. Although conventional optical fibers behave as insulators, the link between the imaginary component of the dielectric function and the frequency-dependent electrical conductivity

$\sigma(\omega)$ underscores the intrinsic connection between a material's optical and electrical behavior. This relationship becomes particularly significant in specialized systems or high-field applications.

Figure 3 (d) shows the computational dielectric function $\varepsilon(\omega)$ for LiNbO₃. This function is complex, consisting of a real part, $\varepsilon_1(\omega)$, which quantifies the material's ability to store energy, and an imaginary part, $\varepsilon_2(\omega)$, which relates to energy absorption.

At low photon energies, $\varepsilon_1(\omega)$, exhibits a relatively high static value (6), reflecting the strong polarizability of LiNbO₃ associated with its ferroelectric nature. The prominent peak in $\varepsilon_1(\omega)$, at 4.02 eV indicates strong

electronic polarization near the fundamental absorption edge. Correspondingly, $\varepsilon_2(\omega)$, shows its first major peak at 5.06 eV, marking the onset of significant interband transitions, primarily from O-2p valence states to Nb-4d conduction states.

In the intermediate energy range (6–20 eV), both $\varepsilon_1(\omega)$, and $\varepsilon_2(\omega)$ display multiple oscillations, arising from transitions involving deeper valence bands and higher-lying conduction bands. The negative values of $\varepsilon_1(\omega)$ observed near 8–10 eV suggest metallic-like response and strong screening, often associated with plasmonic effects.

At higher energies (>30 eV), $\varepsilon_2(\omega)$ approaches zero, indicating diminished absorption, while $\varepsilon_1(\omega)$ gradually stabilizes, reflecting reduced electronic response. Overall, the dielectric spectrum highlights the complex electronic structure of LiNbO₃ and underpins its strong optical activity and suitability for nonlinear and optoelectronic applications.

Figure 3 (e) represents the computational conductivity, $\sigma(\omega)$, of the LiNbO₃, which describes its ability to conduct an electric current. The graph displays the conductivity's real and imaginary components. In the low-energy region, real part remains nearly zero, confirming the insulating nature of LiNbO₃ and its wide band gap, which is essential for low-loss signal transmission in fiber-optic systems. A prominent peak in real part at 5.18 eV marks the onset of strong interband transitions, primarily involving O-2p to Nb-4d electronic excitations. These transitions contribute to optical modulation and electro-optic activity rather than free-carrier absorption.

The imaginary component exhibits a pronounced negative minimum at 4.22 eV, indicating strong capacitive response and phase delay between the electric field and induced current. The subsequent zero crossing and positive peak near 5.95 eV reflect resonant polarization effects linked to electronic transitions. At higher energies (30–40 eV), both parts show sharp features associated with plasmonic and high-energy interband excitations.

The Energy Loss Function ($L(\omega)$), determined by Equation 5, describes how energy is dissipated when light interacts with the fiber material. The following expression is used to determine the energy loss function [34-35]:

$$L(\omega) = -\text{Im}(1/\varepsilon(\omega)) = \varepsilon_2(\omega)/(\varepsilon_1(\omega)^2 + \varepsilon_2(\omega)^2) \quad (5)$$

Although it is not a direct design parameter like the refractive index, the dielectric function provides essential insight into intrinsic loss mechanisms, including ultraviolet absorption arising from interband electronic transitions and infrared absorption associated with lattice vibrations (phonons). A thorough understanding of this function supports accurate material characterization and aids in the development of optical fibers with reduced inherent losses.

Figure 3 (f) illustrates the calculated energy loss function, $L(\omega)$, for Lithium niobate as a function of photon energy. This function represents the energy dissipated by a high-velocity electron traversing the material. Distinct peaks in the spectrum correspond to the excitation of collective electron oscillations, commonly referred to as plasmons.

At low energies (< 5 eV), the loss function is nearly zero, indicating minimal energy dissipation and weak collective excitations, consistent with the insulating and wide-band-gap nature of LiNbO₃. As the energy increases, small features appear in the 5–20 eV range, arising from interband electronic transitions that contribute weakly to energy loss.

A dominant and sharp peak is observed at 25.65 eV, with a maximum value of 3.68, corresponding to the bulk plasmon resonance of LiNbO₃. This energy coincides with the zero-crossing of the real part of the dielectric function, confirming the collective oscillation of valence electrons against the ionic background. The sharpness of this peak reflects well-defined plasmon modes and strong electronic coherence.

Beyond 30 eV, the loss function decreases rapidly, followed by additional pronounced peaks in the 35–40 eV region. These features are associated with higher-energy plasmon modes and interband transitions involving deeper core and semi-core states. At energies above 45 eV, the loss function approaches zero, indicating reduced electron–energy loss processes.

In conclusion, the computational findings suggest that Lithium niobate is a promising candidate for next-generation fiber-optic components. Its distinctive material characteristics—especially those governing nonlinear optical (NLO) behavior—make it well suited for applications such as ultrafast lasers and advanced waveguiding systems. These NLO effects originate from the nonlinear dependence of induced polarization on the applied electric field, with the material's strong third-order susceptibility playing a pivotal role in enabling such high-performance photonic applications. The polarization response can be expressed as a power series in the electric field strength, encompassing both linear and nonlinear effects [35]:

$$P(t) = \varepsilon_0(\chi^{(1)}E(t) + \chi^{(2)}E^2(t) + \chi^{(3)}E^3(t) + \dots) \quad (6)$$

Here, $\chi^{(n)}$ is the nth order nonlinear susceptibility tensor that describes the material's reaction at each order of

nonlinearity, and ϵ_0 is the vacuum permittivity. While higher-order terms relate to nonlinear phenomena like second-harmonic generation ($\chi^{(2)}$) and third-order ($\chi^{(3)}$) processes, such as intensity-dependent refractive index changes and saturable absorption, the first term, $\chi^{(1)}E(t)$, indicates linear optical response.

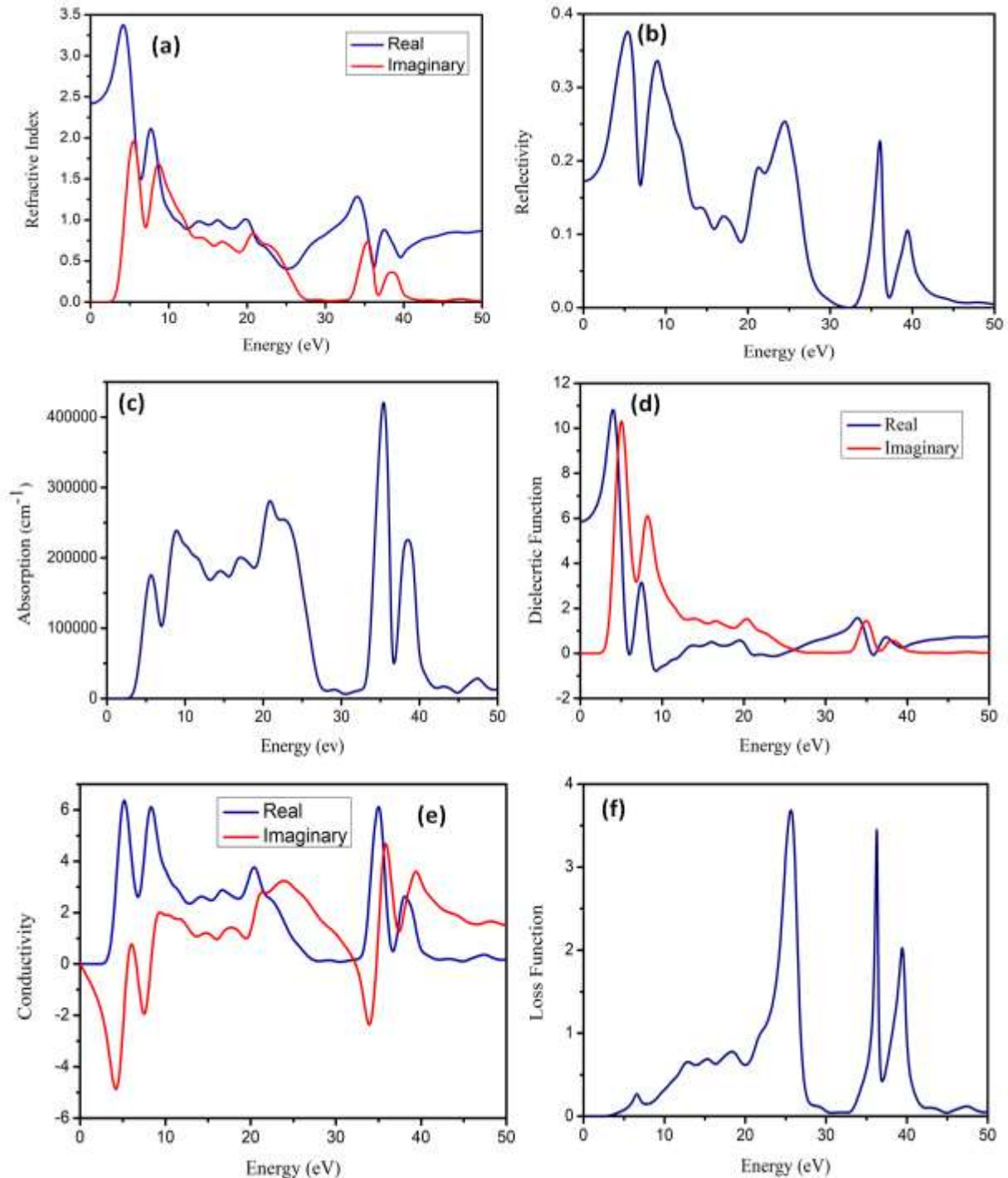


Figure 3. The optical properties of the LiNbO₃ as a function of incident photon energy. The figure (a) the real and imaginary parts of the refractive index, (b) reflectivity, (c) absorption coefficient, (d) the real and imaginary parts of the dielectric function, (e) the real and imaginary parts of the conductivity, and (f) the electron energy loss function.

The linear dielectric function components, $\varepsilon_1(\omega)$ and $\varepsilon_2(\omega)$, describe the material's energy storage and dissipation capabilities in relation to the incident light field. These quantities are related to the linear susceptibility by [34-35]:

$$\varepsilon(\omega) = \varepsilon_1(\omega) + i\varepsilon_2(\omega) = 1 + \chi^{(1)}(\omega) \quad (7)$$

Where, ω is the angular frequency of the light. The refractive index $n(\omega)$ and absorption coefficient $\alpha(\omega)$, which are crucial factors for simulating nonlinear optical behavior, can be easily obtained from $\varepsilon(\omega)$.

Essential NLO effects, such as the nonlinear refractive index n_2 , which characterizes intensity-dependent phase modulation, and nonlinear absorption coefficients pertinent to two-photon absorption and saturable absorption, are governed by the third-order nonlinear susceptibility ($\chi^{(3)}$). The refractive index can be expressed as [35]:

$$n = n_0 + n_2 I \quad (8)$$

Where, n_0 is the linear refractive index and I is the optical intensity. The nonlinear polarization arising from ($\chi^{(3)}$) effects the propagation of high-intensity light pulses in photonic devices such as modulators and optical switches.

Figure 3(a) illustrates that the refractive index, which determines the propagation of light within the material, exhibits its real part reaching a maximum near 3.37 eV, indicating strong light-matter interaction in the visible region. The imaginary component (extinction coefficient) shows a broad peak spanning 2–10 eV, reflecting substantial optical absorption arising from electronic transitions associated with the linear dielectric response (first-order susceptibility). In Figure 3(b), reflectivity increases sharply below 6 eV and subsequently decreases, implying that Lithium niobate strongly reflects visible light while becoming comparatively more transparent at higher photon energies, an aspect critical for optical device applications. Meanwhile, the absorption coefficient in Figure 3(c) rises rapidly and attains a maximum value of approximately $4.2 \times 10^5 \text{ cm}^{-1}$ at around 35.41 eV, emphasizing pronounced interband transitions important for photovoltaic and nonlinear optical functionalities.

The dielectric function, $\varepsilon(\omega)$, directly related to the linear susceptibility (Equation 7), characterizes the interaction of the material with electromagnetic radiation. As shown in Figure 3(d), the real part (ε_1) remains positive at lower energies, signifying energy storage through polarization, but decreases beyond 5 eV. The imaginary part (ε_2) exhibits a prominent peak near 4.02 eV, corresponding to energy dissipation due to electronic excitations. Furthermore, Figure 3(e) demonstrates that the optical conductivity presents notable peaks within the 4–10 eV range, indicating enhanced photo-induced charge carrier dynamics. These conductivity characteristics, together with significant variations in refractive index and absorption, may be further influenced by nonlinear effects proportional to $\chi^{(3)}$ at higher light intensities, thereby impacting phenomena such as optical limiting and self-focusing.

Table 1 illustrates the broad spectrum of LiNbO₃ research, encompassing computational studies of LiNbO₃/LiNbO₃ like. Overall, the material's importance in fiber optics is shown in Table 1, which also shows that it is a suitable nonlinear optical material because of its advantageous refractive index and dielectric constant, which promote effective light propagation and nonlinear optical effects.

Table 1: Optical properties of LiNbO₃ and its applications

Material	Refractive index (n)	Dielectric constant (ε_1)	Band Gap	Application	Ref.
CH ₃ NH ₃ PbI ₃	2.64	7.26	1.7 eV	Fiber optics	[35]
CH ₃ NH ₃ PbI ₃	1.95	3.8	Not specified	Ultrafast photonics	[36]
LiNbO ₃	3.47	9.80	3.54	Modern technologies	[37]
LiNbO ₃	3.37	10.81	3.60	Nonlinear optics	This work

4. CONCLUSION

First-principles calculations were employed to systematically investigate the electronic and optical properties of LiNbO₃, aiming to elucidate its suitability for optoelectronic and nonlinear optical applications. The calculated electronic band structure reveals that LiNbO₃ is a wide-band-gap semiconducting material, with no bands crossing the Fermi level. A clear separation between the valence and conduction bands is observed, where the valence band is dominated by relatively flat O-2p states, indicating localized electronic behavior, while the more dispersive Nb-4d conduction bands suggest enhanced charge mobility upon excitation. The total density of states further confirms the insulating nature of LiNbO₃, with zero DOS at the Fermi level and prominent peaks corresponding to flat band regions.

The optical response was analyzed through the complex refractive index derived from the dielectric function. LiNbO₃ exhibits a high real refractive index in the low-energy region, reflecting strong light–matter interaction in the transparent window. A maximum refractive index of 3.37 near the absorption edge indicates strong polarization. The imaginary part remains negligible at low energies, confirming minimal absorption, while a pronounced peak around 5.34 eV arises from interband electronic transitions. At higher energies, oscillatory features reflect multiple electronic excitations, and absorption diminishes beyond 30 eV. Overall, these results provide a comprehensive understanding of the electronic structure and optical behavior of LiNbO₃, supporting its importance in photonic and fiber-optic technologies.

Conflict of Interests

The authors declare that they have no conflict of interest.

Credit Author Contribution

Dr. Mulayam Singh Patel: Writing-original draft, Review and editing, Data curation, Investigation, Validation, Software, Supervision, **Priyanka Singh:** Writing-original draft, Formal analysis, Validation

REFERENCES

- 1) Boyd, R. W. *Nonlinear Optics*. Academic Press, 2008.
- 2) Weis, R. S., and Gaylord, T. K. "Lithium niobate: Summary of physical properties and crystal structure." *Applied Physics A* 37 (1985): 191–203.
- 3) Wang, X. et al. "Electronic structure and optical properties of LiNbO₃." *Journal of Applied Physics* 97 (2005): 046105.
- 4) Abrahams, S. C. et al. "Ferroelectric lithium niobate. Crystal structure." *Journal of Physical Chemistry Solids* 27 (1966): 997–1012.
- 5) Sanna, S. et al. "First-principles investigation of defect energetics in LiNbO₃." *Physical Review B* 86 (2012): 144117.
- 6) Gayer, O. et al. "Temperature and wavelength dependent refractive index equations for MgO-doped and congruent LiNbO₃." *Applied Physics B* 91 (2008): 343–348.
- 7) Choi, S. Y. et al. "Electro-optic properties of lithium niobate single crystals." *Optics Letters* 40 (2015): 2004–2007.
- 8) Pati, R. K. et al. "DFT study of optical conductivity and dielectric behavior in LiNbO₃." *Materials Chemistry and Physics* 210 (2018): 231–239.
- 9) Chen, X. et al. "Lithium niobate photonics for microwave-to-optical conversion." *Nature* 568 (2019): 373–377.
- 10) Boes, A. et al. "Lithium niobate photonics: status and prospects." *APL Photonics* 6 (2021): 010901.
- 11) Guarino, A. et al. "Electro-optically tunable microring resonators in lithium niobate." *Nature Photonics* 1 (2007): 407–410.
- 12) Wang, C. et al. "Integrated lithium niobate electro-optic modulators." *Optica* 5 (2018): 1438–1441.
- 13) Luo, R. et al. "Critical role of optical loss in integrated lithium-niobate modulators." *Laser & Photonics Reviews* 13 (2019): 1800288.
- 14) Chang, L. et al. "Heterogeneously integrated lithium niobate photonics." *Optica* 3 (2016): 531–535.
- 15) Jin, H. et al. "On-chip generation and manipulation of entangled photons using LiNbO₃." *Physical Review Letters* 113 (2014): 103601.
- 16) Lu, J. et al. "Universal frequency comb generation in thin-film lithium niobate." *Nature Physics* 15 (2019): 373–381.
- 17) Yuan, Z. et al. "Optical absorption behavior of LiNbO₃ under UV irradiation." *Journal of Luminescence* 218 (2020): 116802.
- 18) Li, Y. et al. "Band-gap engineering in doped LiNbO₃ for nonlinear optical applications." *Ceramics International* 47 (2021): 13845–13853.
- 19) Xie, H. et al. "Waveguide engineering in lithium niobate for low-loss transmission." *Optics Communications* 465 (2020): 125563.
- 20) Tien, M. C. et al. "Silicon–lithium niobate hybrid integration for optical links." *Optics Express* 23 (2015): 25521–25527.
- 21) Zhang, Q. et al. "Thin-film LiNbO₃ modulators for terahertz communications." *IEEE Journal of Quantum Electronics* 57 (2021): 1–8.
- 22) Lin, J. et al. "Broadband optical control using LiNbO₃ for quantum photonics." *Light: Science & Applications* 10 (2021): 73.

- 23) Rao, S. et al. "Improvement of optical transparency in lithium niobate via defect control." *Journal of Alloys and Compounds* 777 (2019): 93–101.
- 24) Chen, Z. et al. "Absorption coefficient mapping of LiNbO₃ thin films." *Thin Solid Films* 693 (2019): 137673.
- 25) Kenda, A. et al. "Dielectric spectroscopy of lithium niobate crystals." *Solid State Communications* 260 (2017): 13–18.
- 26) Nakamura, K. et al. "Optical conductivity of ferroelectric LiNbO₃." *Ferroelectrics* 530 (2018): 102–110.
- 27) He, L. et al. "High-performance electro-optic fiber couplers using LiNbO₃." *IEEE Photonics Technology Letters* 30 (2018): 1190–1193.
- 28) Sun, J. et al. "LiNbO₃-based integrated photonics for fiber-optic communication." *Journal of Lightwave Technology* 39 (2021): 1276–1287.
- 29) Rao, S. et al. "Improvement of optical transparency in lithium niobate via defect control." *Journal of Alloys and Compounds* 777 (2019): 93–101.
- 30) Zhao, X. et al. "Plasmon resonance effects in LiNbO₃ nanostructures." *Optics Express* 28 (2020): 35650–35661.
- 31) Fujimura, M. et al. "Nonlinear optical response of lithium niobate for photonic switching." *Optics and Laser Technology* 132 (2020): 106493.
- 32) Lin, J. et al. "Broadband optical control using LiNbO₃ for quantum photonics." *Light: Science & Applications* 10 (2021): 73.
- 33) Rawat R. K. et al. "Understanding H₂ adsorption on mesoporous SnO₂ nanospheres: a combined DFT and experimental study" *Phys. Scr.* 100 (8) (2025) 085003.
- 34) Ghani M. U. et al. "CASTEP investigation of structural, electronic, and optical properties of halide perovskites RbXCl₃ (X = Ge, Sn, Pb) for solar cell applications, *Inorg. Chem. Commun.* 155 (2023) 111007.
- 35) Patel M. S. et al. "Experimental and computational investigation of CH₃NH₃PbI₃ material for next-generation fiber optic applications" *Chemistry of Inorganic Materials* 7 (2025) 100129.
- 36) Li P. et al "Two-Dimensional CH₃NH₃PbI₃ perovskite nanosheets for ultrafast pulsed fiber lasers" *ACS Appl. Mater. Interfaces* 9 (14) (2017) 12759–12765.
- 37) Hossain Md. M. "First-principles study on the structural, elastic, electronic and optical properties of LiNbO₃" *Heliyon* 5 (2019) e01436.